Journal of Tropical Resources and Sustainable Science
Website : http://journal.umk.edu.my/index.php/jtrss/
eISSN : 2462-2389
Vol: 14, Issue 1, 2026, 158-167
DOI: https://doi.org/10.47253/jtrss.v14i1.2170

RESEARCH ARTICLE

Noise Level Study of Hair Dryer with Perforated Absorber

Hui Ni Tan[1], Lu Ean Ooi[1*], Choe Yung Teoh[2] Keng Wai Chan[1]

[1]School of Mechanical Engineering, Universiti Sains Malaysia, Engineering Campus, 14300 Nibong Tebal, Penang, Malaysia
[2]Faculty of Engineering and Technology, Tunku Abdul Rahman University of Management and Technology, 53300 Kuala Lumpur, Malaysia

ARTICLE HISTORY
Received : 16 August 2025
Accepted : 10 November 2025
Online : 31 March 2026

KEYWORDS
perforated panel,
noise level,
sound absorber,
additive manufacturing,
PLA material

☒ * **CORRESPONDING AUTHOR**
Dr. Ooi Lu Ean
School of Mechanical Engineering,
Universiti Sains Malaysia,
Engineering Campus, 14300 Nibong
Tebal, Penang, Malaysia
Email: ooiluean@usm.my

ABSTRACT

As user expectations for comfort and product quality increase, reducing noise from household appliances like hair dryers has become increasingly important. This study investigates the effectiveness of a perforated sound absorber in reducing noise emitted by a 2100W commercial hair dryer. The initial acoustic characterization was performed by measuring the overall sound power level (SWL) using a hemispherical microphone array, in accordance with ISO 3742. To identify the dominant noise source, Microflown Scan & Paint technology was employed, revealing the air inlet as the primary noise source. A perforated sound absorber was designed to be mounted at this location. Key design parameters–perforation diameter, panel thickness, perforation ratio, and air cavity depth–were optimized using sound absorption coefficient (SAC) simulations. The simulation model was validated through experimental measurements using a standard two-microphone impedance tube setup in accordance with ASTM E1050-98. The optimized design was fabricated via fused deposition modeling (FDM) using PLA and installed at the air inlet of the hair dryer. Subsequent SWL measurements indicated a noise reduction of 2.15 dB(A) compared to the hair dryer without the attachment, confirming the absorber's potential for targeted noise control.

1. INTRODUCTION

Noise is generally defined as any unwanted or disruptive sound originating from natural or human-made sources. Sound levels between 120 to 130 dB SPL can cause physical pain and immediate harm to the human ear, which is commonly referred to as the threshold of pain (István and Leo, 2005). However, even below this threshold, prolonged exposure to elevated noise levels can be harmful. The National Institute for Occupational Safety and Health (NIOSH) recommends a maximum exposure limit of 85 dB(A) over an 8-hour workday (NIOSH, 1998). Exposure to such noise levels over extended periods has been associated with serious health risks, including permanent hearing loss, hypertension, cardiovascular issues, sleep disturbances, and heightened stress levels (Münzel et al., 2014). As consumer expectations for household appliances continue to rise, the focus has shifted from basic functionality to user comfort and overall product quality. Hair dryers, as common personal care devices, are increasingly evaluated not only based on power output, heat settings, and design features–such as ceramic technology or ionization–but also in terms of their acoustic footprint. Although often overlooked, noise can be a decisive factor for users with auditory sensitivity. According to the Hairdressers Journal, individuals with autism are particularly sensitive to high noise levels, making quieter operation a significant aspect of inclusive product design. Typical hair dryers generate sound pressure levels ranging from 80 to 90 dB(A), which may exceed comfort thresholds for many users.

In response to growing concerns about acoustic performance, numerous patents have been issued for noise mitigation strategies in hair dryers. For instance, Altamore proposed a muffler-integrated hair dryer design that reduces noise by incorporating absorptive elements at the inlet while preserving airflow at the outlet (Nicolo, 1999). Similarly, Rodrigues introduced a noise reducer positioned at the rear air entrance, using phono-absorbent material to dissipate incoming sound energy (Rodrigues, 2010). The dominant source of noise in hair dryers is the internal fan motor (Lahaye, 2022), which produces both mechanical and aerodynamic noise. Mechanical noise stems from structural vibrations, whereas aerodynamic noise arises from turbulent flow interactions with internal components such as grills, heaters, and filters. Experimental findings by Akhmetov et al. (2014) revealed the concentration of jet mixing noise at a 20° angle relative to the airflow direction, corresponding to the area directed toward the user's ear. The study further emphasized

the influence of internal structures like air filters and casing materials on the overall acoustic signature. The attenuation performance is intrinsically tied to the geometric and material properties of components like the fan blades, motor mounts, and diffuser grills (Huang and Zheng, 2022). Gupta et al. (2014) demonstrated the effectiveness of bulk absorptive liners and Helmholtz resonators in reducing fan tones and broadband noise. Their approach achieved up to 12 dB attenuation in targeted frequency ranges, though it required significant structural volume and design modifications. Lahaye (2022) examined passive noise mitigation techniques in hair dryers, including porous linings and micro-perforated panels (MPPs), revealing that MPPs with porous backing cavities can outperform conventional materials at specific frequencies. Che et al. (2024) extended this work through optimization of nozzle geometries, reducing perceived sound levels by up to 15% using refined outlet shapes. Despite these advances, few studies or patents have explored the integration of micro-perforated panels directly into the intake of the hair dryer, where fan-generated noise first emerges.

The MPP is a promising passive acoustic solution characterized by a thin plate embedded with sub-millimeter holes (typically <1 mm), uniformly distributed to maximize viscous loss mechanisms. Its absorption performance spans broad frequency ranges and is governed by key design parameters: hole diameter (d), panel thickness (t), perforation spacing (b), and backing air gap depth (D). Various materials including metals, polymers, and composites have been used to fabricate MPPs (Herrin and Liu, 2011; Liu et al., 2017; Qian et al., 2013; Sakagami et al., 2021; Wareing et al., 2015). Earlier designs used laser-perforated metal sheets (Herrin et al., 2017), while more recent advances in micro-electromechanical systems (MEMS) have allowed fabrication at sub-micron precision (Liu et al., 2017). However, both approaches remain cost-prohibitive for consumer applications. Additive manufacturing, especially 3D printing, offers a low-cost and versatile alternative. Several studies (Carbajo et al., 2024; Gao & Hou, 2018; Liu et al., 2017) have demonstrated the viability of stereolithography (SLA) for producing MPPs with high geometric precision. Others have successfully utilized fused deposition modelling (FDM) using polylactic acid (PLA), showing that performance remains consistent with theoretical predictions (Gao & Hou, 2018; Mohamed Shafeer et al., 2024; Sailesh et al., 2021; Sailesh et al., 2022). In this study, FDM printing was selected for its affordability, lightweight material compatibility, and ease of iterative prototyping.

The present work investigates a perforated sound absorber specifically designed specifically for hair dryers. The study begins with identification of dominant noise sources through spatial sound mapping, followed by acoustic simulation to identify optimal MPP parameters. A small-scale sample was fabricated and validated using impedance tube measurements to ensure good agreement between predicted and measured sound absorption characteristics. Based on the validated design, an MPP based sound absorber was integrated at the air inlet of the hair dryer to target noise generated by the internal motor. Sound levels were then measured across four usage configurations, with and without the absorber, to quantify its performance. The results demonstrate the perforated sound absorber's effectiveness in attenuating noise intake, offering a lightweight, passive noise control solution without compromising device functionality.

2. METHODOLOGY

2.1. Study process

To evaluate the effectiveness of a micro-perforated panel (MPP) as a noise reduction solution for a commercial hair dryer, this study employed a combination of experimental measurements, sound field visualization, and numerical simulation. The investigation began by determining the original acoustic characteristics of the hair dryer through standardized sound power level (SWL) measurements. These measurements were complemented by acoustic mapping to identify the primary noise radiation zones. The results informed the targeted design of an MPP absorber using simulation software. The optimized MPP was subsequently fabricated via 3D printing and installed on the hair dryer. Post-installation measurements were then conducted to assess the improvement in acoustic performance. This integrated approach ensured both empirical validation and design optimization.

2.2. Determination of Sound Level

The overall SWL of the hair dryer was measured using a hemispherical microphone array in accordance with ISO 3742 standards and B&K Application Note BO 0416-12, as shown in Figure 1. A commercial hair dryer rated at 2100 W served as the test subject. The hair dryer came with several attachments, including a ThermoProtect attachment, a styling nozzle, and a diffuser. Measurements were conducted in hot mode to reflect realistic operational conditions and to capture noise contributions from the heating element, which intensifies acoustic emissions (Akhmetov et al., 2014; Che et al., 2024). All measurements were conducted at both low and high fan speeds, with each of the attachments and without any attachment. The measurement setup included LMS Scadas Mobile hardware, eight GRAS 46AD microphones, a BSWA MF710 hemispherical array (with a radius of 1 meter), and a

laptop running LMS Test.Xpress software. The microphones were calibrated and evenly positioned on the hemispherical frame surrounding the test point. Then, they were connected to the data acquisition (DAQ) device. The DAQ device was connected to the laptop. The hair dryer was mounted at the geometric center using a retort stand, with care taken to maintain consistent orientation and distance during all measurements. The microphones captured sound data, which were processed to determine the overall SWL both before and after the implementation of the perforated sound absorber.

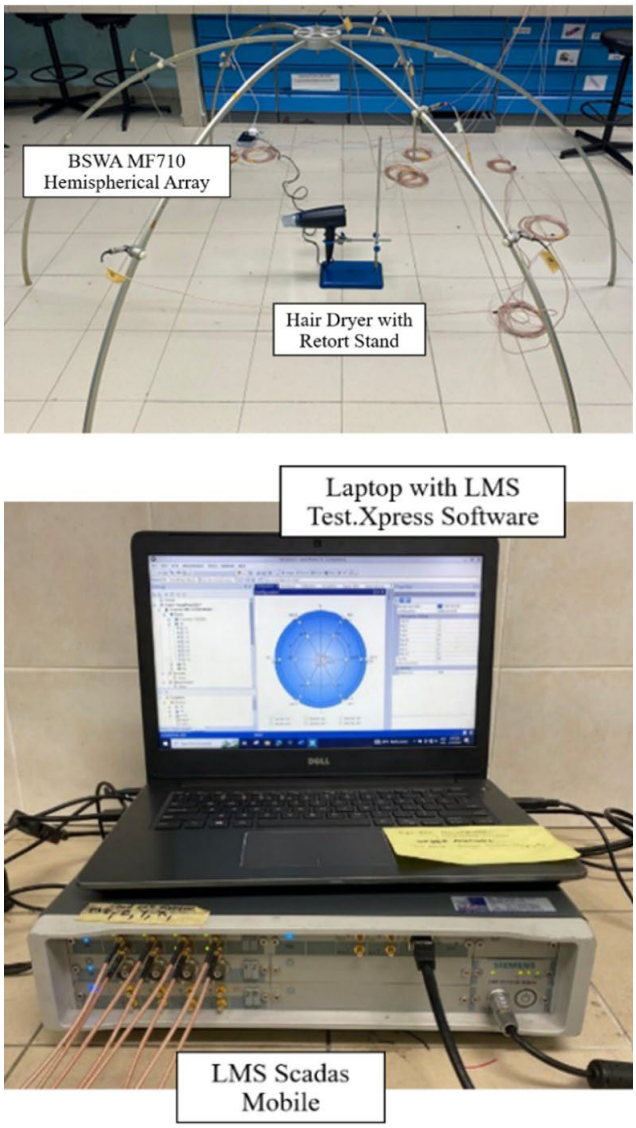

Figure 1: Sound level measurement experimental setup

To localize and visualize the primary noise radiation zones of the hair dryer, sound field characterization was performed using Microflown Scan & Paint Technology. This measurement technique enabled the acquisition of both sound pressure and particle velocity data, facilitating a detailed acoustic mapping of the device. The experimental setup consisted of a PU (pressure-velocity) probe, a two-channel signal conditioner, a data acquisition (DAQ) interface, a laptop equipped with Microflown Scan & Paint software, a camera mounted on a tripod, and a retort stand used to position the hair dryer, as illustrated in Figure 2. The PU probe was systematically scanned across the surface of the hair dryer to measure the acoustic particle velocity and sound pressure at discrete locations. To ensure the accuracy of the captured data, the probe was held as close as practicable to the hair dryer surface without physical contact. This proximity minimized spatial averaging effects and captured the near-field characteristics essential for localizing true source regions. The scanning process was carried out incrementally on all exposed surfaces of the hair dryer, including the front outlet, rear inlet, and both lateral sides. This was done to ensure complete spatial coverage. Concurrently, the camera, positioned directly in front of the hair dryer, captured the image of the scanned surface, enabling the software to overlay the measured acoustic data onto the corresponding geometry in real time. The resultant sound maps provided visual representations of the dominant noise-emitting zones, which were later used to inform the strategic placement and design of the MPP-based sound absorber.

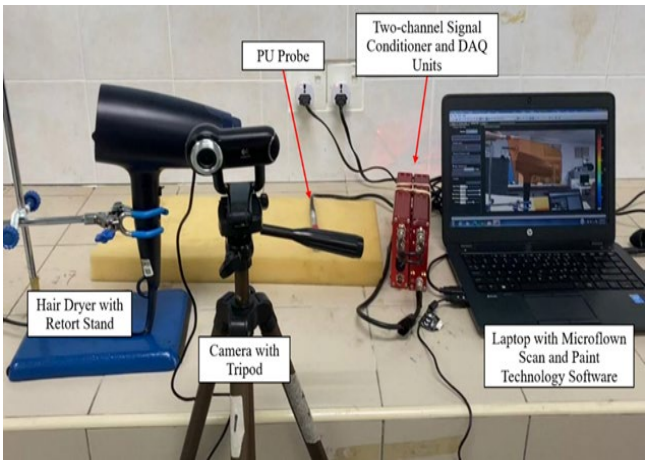

Figure 2: Sound mapping measurement experimental setup

After identifying the sound source location, a perforated absorber made from MPP was designed to be installed at the primary noise source of the hair dryer. The parameters of the perforated absorber, such as the perforation diameter, plate thickness, perforation ratio, and air cavity, were determined based on the design constraints. The simulated sound absorption coefficients (SACs) of MPPs with varying geometric configurations were compared to identify the optimal design capable of achieving high absorption performance in the frequency range associated with the hair dryer's noise emissions. A set of candidate MPP configurations was selected, each with slight variations in perforation diameter, panel thickness, and air cavity depth, while maintaining manufacturability via additive techniques. The SAC values obtained from boundary element simulation were cross-validated with experimental results from an

impedance tube test, using a small-scale MPP sample fabricated based on one of the simulated configurations. For the simulation, the acoustical simulation model was created using SolidWorks software by sketching a CAD 3D model. The model was designed to simulate the actual conditions of the SAC measurement using an impedance tube. The dimensions of the model were based on the dimensions of the actual impedance tube and MPP, which were sketched in Figure 3. The main tube of the impedance tube was cylindrical in shape, with an inner diameter of 34.8 mm and a length of 850 mm. The acoustical simulation model was imported to conduct the SAC simulation. The SAC of the MPPs with different parameters was simulated. In this simulation, the acoustic material was air with its standard properties. The noise source was set at the inlet of the impedance tube with an acoustic panel normal velocity of 1 m/s. The sound pressure recorded from the two microphones was shown in both real and imaginary forms through the simulation. The sound pressure data from each microphone was exported, and the SAC was calculated using Matlab software.

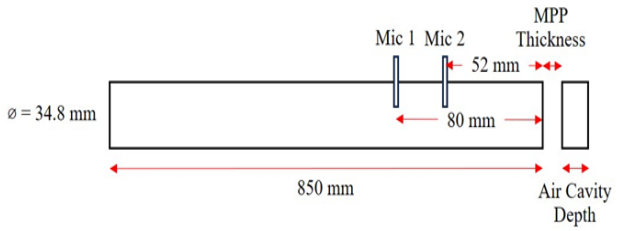

Figure 3: Dimension used on boundary elements simulation model

2.3. Experiment Measurements and Validation

The MPP sample incorporating the optimized parameters was fabricated using a FlashForge Guider 2 3D printer, employing fused deposition modelling (FDM) technology and polylactic acid (PLA) filament as the printing material. PLA was selected due to its favorable acoustic rigidity, cost-effectiveness, and compatibility with FDM printing. Following the 3D printing process, a post-processing step was carried out to enhance the precision of the micro-perforations. Although the overall structure was printed with high resolution, the perforations were manually refined using precision drill bits to achieve the intended diameter and ensure geometric consistency across the panel. This manual drilling process was necessary to compensate for the limitations of the FDM printing resolution in producing sub-millimeter holes. The final diameter of the printed sample was 34.8 mm, precisely matching the inner diameter of the impedance tube, thus ensuring a snug fit and eliminating the potential for air leakage during acoustic measurements. The specific dimensions of the perforations—namely the hole diameter and the center-to-center spacing—were configured according to the selected MPP design parameters derived from the simulation stage. A schematic of the fabricated MPP sample is provided in Figure 4, detailing the geometric configuration used for both simulation and experimental validation.

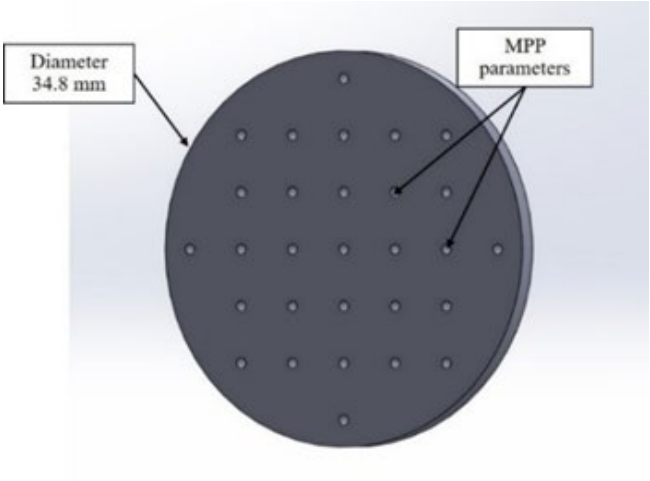

Figure 4: Small scale MPP sample ready for 3D printing

To validate the simulated SAC results, experimental measurements were conducted using a standard two-microphone impedance tube method in accordance with ISO 10534-2 and ASTM E1050-98 standards. The SAC of the MPP samples fabricated with the selected parameters was measured using the impedance tube with an inner diameter of 34.8 mm. The experimental setup was illustrated in Figure 5 and comprised the following equipment: an LMS Scadas data acquisition (DAQ) system, two GRAS 46AD condenser microphones, the impedance tube apparatus, and a laptop operating LMS Test.Lab Sound Absorption Testing software.

The two microphones were positioned upstream of the MPP sample at fixed locations, with the separation distance carefully calibrated to ensure compliance with the standards for accurate SAC computation. Prior to the actual measurements, the system was calibrated using a standard sponge material to verify the reliability of the setup. Following calibration, the 3D-printed MPP sample was inserted into the designated sample holder and securely locked in place at the termination end of the tube. The termination piston was adjusted to define the air cavity depth according to the optimized MPP design parameters. During testing, a known broadband sound signal was generated at the source end of the tube. Microphone 1 captured the incident sound waves, while Microphone 2 recorded the reflected waves. These measurements were processed by the software to compute the SAC over the frequency range of interest. The experimentally obtained SAC results were subsequently compared with the simulated SAC to assess the accuracy and reliability of design parameters.

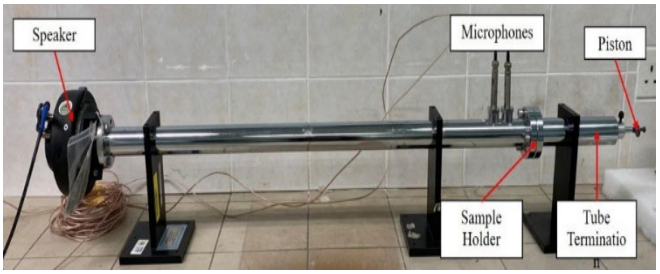

Figure 5: Impedance tube experimental setup

2.4. Design and Fabrication of Perforated Absorber

Following the identification of optimal acoustic parameters through simulation, the micro-perforated panel (MPP) was fabricated using additive manufacturing. The final design incorporated key parameters–perforation diameter, panel thickness, and air cavity depth–which were determined from the validated SAC simulation. The MPP model was initially constructed in SolidWorks CAD software and exported as a stereolithography (STL) file, compatible with the 3D printing platform. Fabrication was carried out using a FlashForge Guider 2 desktop 3D printer employing Fused Deposition Modeling (FDM) technology. Polylactic acid (PLA) filament was selected as the build material due to its acoustic suitability, ease of post-processing, and favorable cost-performance ratio. The print settings included a 100% infill density to ensure maximum structural integrity and acoustic fidelity, and a print speed of 60% of the printer's nominal capacity to enhance dimensional accuracy.

To improve print quality and facilitate post-processing, the MPP design was modularized into three distinct components: (1) an adapter, functioning as a structural interface between the MPP and the hair dryer casing; (2) a perforated plate, which acts as the primary sound absorber; and (3) an air cavity section that provides the necessary backing depth for resonance tuning. Figure 6 shows the three individual components and the assembled unit. This segmented design approach offered significant advantages by eliminating the need for support structures during printing and simplifying the finishing processes. Post-fabrication, the perforated plate was refined to ensure the precision of the micro-holes. Although the 3D printer produced visible perforations, a finishing step was applied by manually drilling each hole using a bit corresponding to the target perforation diameter (0.8 mm). This step ensured uniform hole geometry and consistency across the entire plate. The thickness of the perforated plate was measured and adjusted to 1 mm, while the air cavity depth was fine-tuned using calibrated sanding of the cavity surfaces. These adjustments were necessary to precisely match the simulated design parameters.

After dimensional validation, the three parts were assembled using cyanoacrylate adhesive (super glue) to form the complete perforated sound absorber unit. The modular fabrication and finishing process enabled precise control over geometric accuracy, which is critical for the acoustic performance of the MPP absorber when integrated into the hair dryer.

Figure 6: 3D printed samples for installation

3. RESULT AND DISCUSSION

To establish a reference for evaluating the noise reduction performance of a perforated sound absorber, the overall SWL of the hair dryer was first measured under various operating conditions prior to any sound absorber implementation. Measurements were conducted at both high and low fan speed settings, with and without the manufacturer-supplied attachments: ThermoProtect attachment, styling nozzle, and diffuser. The sound measurements were performed in hot air mode, as this mode activates the heating element, resulting in higher and more representative noise levels. For each configuration, three repeated measurements were taken to ensure consistency and statistical reliability. The average SWL values for each condition were recorded and are presented in Table 1. At high fan speed, the measured SWL values were 87.38 dBA without any attachment, 86.77 dBA with the ThermoProtect attachment, 86.13 dBA with the styling nozzle, and 87.57 dBA with the diffuser. In contrast, the corresponding measurements at low fan speed were 79.17 dBA (no attachment), 79.34 dBA (ThermoProtect), 78.85 dBA (styling nozzle), and 79.77 dBA (diffuser).

These results indicate that the overall sound level of the hair dryer in high-speed mode is consistently higher than that of low-speed mode across all attachment types. This trend is primarily attributed to the increased power output of the hair dryer's motor at higher fan speeds, which intensifies both aerodynamic and mechanical noise generation. According to previous studies (Azimi and Ommi, 2014; Sathyan et al., 2020), the increased load on the motor leads to greater turbulence and internal airflow, thereby elevating the emitted noise levels.

Among the attachment types, the diffuser produced the highest noise level at both fan speeds (87.57 dBA at high

speed and 79.77 dBA at low speed), likely due to its larger surface area and structural design, which could introduce additional flow disturbances. Conversely, the styling nozzle resulted in the lowest SWL at high speed (86.13 dBA), suggesting it may streamline airflow more efficiently. Given the substantial difference in noise levels between fan speed settings, and the more prominent acoustic emission at high fan speeds, the study focuses primarily on the high-speed operation mode for MPP application. This approach ensures that the designed MPP targets the most acoustically critical operating condition, thereby maximizing the potential impact of the noise reduction treatment.

Table 1: Overall SWL of hair dryer with different attachments (dBA)

Attachments	None	ThermoProtect	Styling nozzle	Diffuser
High speed mode	87.38	86.77	86.13	87.57
Low speed mode	79.17	79.34	78.85	79.77

Figures 7 and 8 present the sound mapping results of the hair dryer under operating conditions without and with a diffuser attachment, respectively. The acoustic maps are displayed from six distinct viewpoints: (a) front, (b) back, (c) top, (d) bottom, (e) left side, and (f) right side. These maps were generated using Microflown, where the color contours represent the spatial distribution of sound levels in decibels (dB). The goal of this analysis is to localize primary noise sources and to assess the effectiveness of the diffuser in modifying the acoustic output of the device. In Figure 7, the acoustic field of the hair dryer without any attachment is characterized by two prominent noise sources: the air intake region and the outlet nozzle, as indicated in Figure 7(a). These areas exhibit high sound levels, exceeding 85 dB(A), denoted by the red and orange contours. The elevated sound radiation at the intake side (Figure 7(c)) is attributed to fan blade rotation and turbulent air suction, while the outlet region (Figures 7(e) and 7(f)) is dominated by jet noise generated by high-velocity airflow impinging on the surrounding environment. Figures 7(b) and 7(d) display side and oblique views, highlighting broader sound dispersion patterns around the body of the dryer, which may be associated with structural vibrations and secondary air interactions. The frontal view in Figure 7(e) and axial nozzle view in (f) reveal a largely symmetrical noise distribution with a peak at the nozzle center, consistent with axisymmetric jet flow behaviour. These observations confirm that both the suction and exhaust mechanisms contribute significantly to the overall acoustic footprint of the device.

Figure 8 illustrates the sound radiation pattern of the same hair dryer fitted with a diffuser attachment at the nozzle. A substantial reduction in sound level is observed at the outlet region across all viewing angles, particularly in Figures 8(a), 8(e), and 8(f). The addition of the diffuser appears to have suppressed high-frequency turbulent components and redirected the flow, resulting in lower noise intensity at the nozzle. In contrast to Figure 7(f), where the sound field is concentrated and intense, the pattern in Figure 8(f) is broader with concentric, less intense contours, suggesting reduced directivity and a shift toward a more diffused acoustic emission. Despite this improvement, the intake side still exhibits considerable noise radiation (Figure 8(c)), although with slightly reduced magnitude compared to the baseline condition. Side and oblique views (Figures 8(b) and 8(d)) demonstrate a more uniform SPL distribution with fewer localized peaks, which may be indicative of less pronounced flow detachment and surface interaction due to the diffuser's aerodynamic effect.

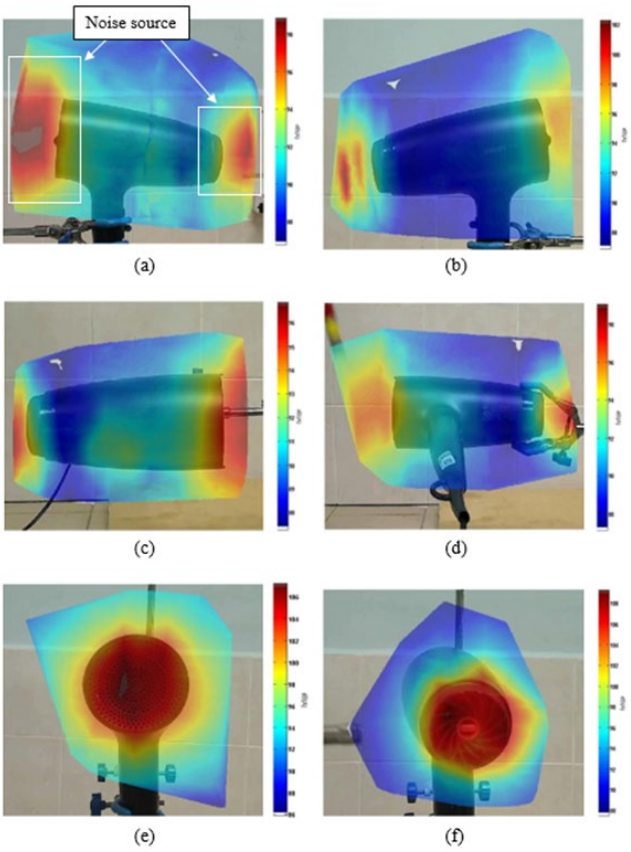

Figure 7: Sound mapping of hair dryer without attachment: (a) front, (b) back, (c) top, (d) bottom, (e) left, and (f) right views.

The figures clearly show that the dominant noise sources of the hair dryer are located at both the air inlet and outlet regions. The acoustic maps for the hair dryer with and without diffuser attachments reveal varying noise source intensities but consistently highlight the air inlet and outlet as principal contributors to the overall noise radiation. The air inlet emerges as a significant noise source due to its proximity to the motor assembly, which is the primary generator of

mechanical and aerodynamic noise. The structural configuration allows noise from the motor to propagate outward more directly through the inlet grille, thereby intensifying the radiated sound levels at that location. Conversely, the air outlet also contributes substantially to noise generation, primarily due to high-velocity turbulent airflow impinging directly on the surrounding medium and, by extension, on the microphone diaphragm. This direct jet flow leads to rapid fluctuations in local pressure, which are detected as elevated noise levels. Such turbulent flow interactions and pressure gradients are well-documented sources of broadband noise in ducted air systems (Cawser, 2019).

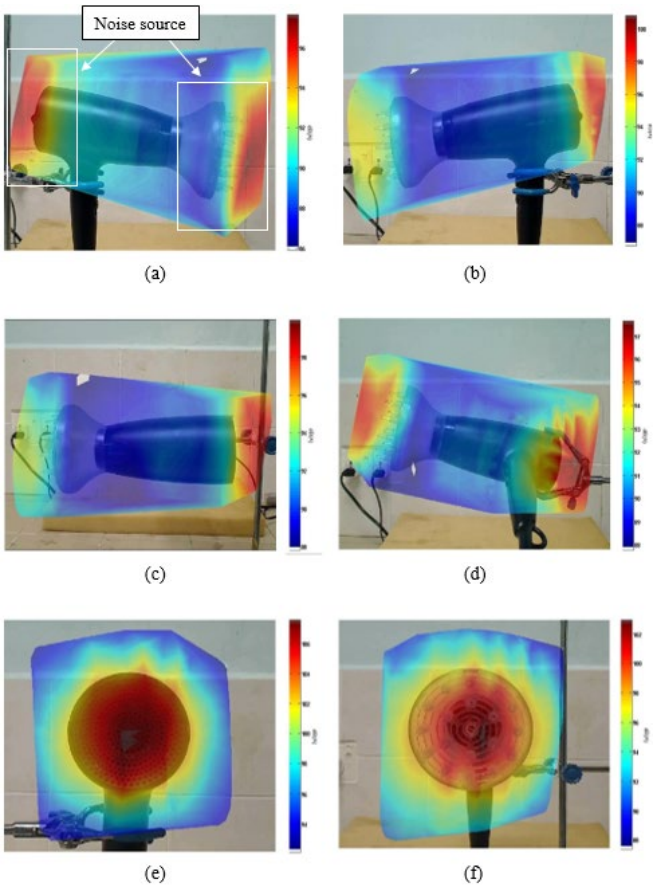

Figure 8: Sound mapping of hair dryer with diffuser: (a) front, (b) back, (c) top, (d) bottom, (e) left, and (f) right views.

While the diffuser attachment has demonstrated effectiveness in attenuating noise radiated from the outlet, as shown in Figure 8, the noise level at the air inlet remains relatively high, with only marginal reduction observed. Given that the outlet side will be physically occupied by functional attachments—such as diffusers or styling nozzles—the practical opportunity for applying additional passive noise treatments at the outlet is limited. As a result, the strategic focus for further noise control shifts toward the air inlet region, which remains exposed and accessible for acoustic treatment. To address this, it is proposed that a tailored sound absorber made with MPP be integrated into the air inlet region of the hair dryer. The sound absorber, when backed by an appropriately dimensioned air cavity, can provide efficient broadband sound absorption without significantly impeding airflow or altering the device's performance. This solution is particularly advantageous due to its compactness, durability, and thermal resistance, making it suitable for integration into the plastic housing or grille structure of consumer hair dryers.

By targeting the air inlet, where structural and flow-induced noise from the motor assembly is most pronounced, the implementation of an MPP-based sound absorber is expected to yield a significant reduction in radiated noise levels. This approach supports a more acoustically optimized product design while preserving the operational efficiency and ergonomic constraints of the hair dryer.

To guide the design of the MPP-based sound absorber and ensure its acoustic effectiveness, a preliminary investigation was conducted to determine the optimal micro-perforated panel parameters. This involved both numerical simulation and experimental validation of the sound absorption performance of a small-scale MPP sample fabricated with different design values. Figure 9 presents a comparison between the simulated and measured sound absorption coefficient of the MPP sample. The selected parameters—perforation diameter, plate thickness, perforation ratio, and air gap—were varied iteratively in the simulation to match the expected noise frequency range of the hair dryer, particularly focusing on the low- to mid-frequency band associated with motor and intake flow noise. The experimental results show good agreement with the simulated absorption profile, particularly around the targeted resonance frequency where peak absorption is desired. Both curves had peak frequencies at around 1400 Hz. However, the SAC values obtained experimentally were higher than those from the simulation across the frequency range. This small deviation may be attributed to inaccuracies in the fabricated MPP parameters. The irregular shape and inconsistent sizes of the perforation holes in the MPP could have affected the accuracy of the SAC measurement (Jafar et al., 2020, Alisah et al., 2021, Jafar et al., 2021). During the additive manufacturing process, such as 3D printing, the layer-by-layer solidification process can lead to the noncircular geometry of the perforation holes. Although manually drilling was performed during the finishing processing, achieving perfectly circular perforation holes remained challenging. In general, both the results from the simulation and experimental data were relatively similar and well correlated. This alignment validates the accuracy of the modelling approach and

confirms that the chosen design parameters are suitable for broadband absorption in the operating frequency range of the hair dryer. Based on this validated result, the same parameters were adopted in the full-scale cylindrical MPP-based absorber integrated into the hair dryer system.

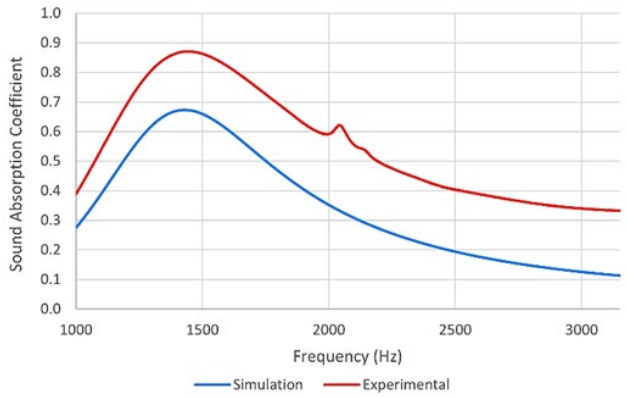

Figure 9: Comparison of measured and simulated SAC

The MPP-based sound absorber implemented in this study was inspired by the cylindrical MPP configuration proposed by Rafique et al. (2022), which demonstrated effective broadband absorption in ducted flow systems. The adopted design features a cylindrical geometry, concentrically positioned around the air inlet perimeter of the hair dryer. This configuration was selected to provide both acoustic attenuation and mechanical compatibility with the existing hair dryer structure. Structurally, the absorber consists of a hollow cylindrical shell that functions as both a support adapter and the carrier of the micro-perforated surface. The central opening in the MPP allows unimpeded airflow into the hair dryer, maintaining its functional airflow performance. Simultaneously, the annular section of the MPP—positioned around the central inlet—acts as a passive absorber, targeting noise emitted from the motor that radiates outward through the inlet path.

The dual-path strategy of this design enables two simultaneous outcomes: (1) the central region facilitates the required airflow for normal dryer operation, and (2) the surrounding micro-perforated section effectively absorbs the engine-generated noise that would otherwise escape through the inlet. The perforations on the MPP panel dissipate acoustic energy via viscous and thermal losses in the narrow apertures and adjacent air cavity. Dimensional specifications of the MPP absorber were guided by practical constraints and acoustic design criteria. The inner diameter of the cylindrical absorber was set to 84.4 mm to match the outer edge of the hair dryer's inlet. The diameter of the central unobstructed hole was fixed at 55 mm, providing a sufficient open area to ensure minimal airflow resistance. The overall thickness of the MPP plate, perforation diameter, perforation ratio, and backing cavity depth were determined based on preliminary simulations and prior parametric optimization studies, ensuring that the MPP would be tuned to absorb the dominant frequencies associated with the motor and intake flow noise. This configuration provides a compact and modular solution for inlet-side noise control, allowing for easy attachment and potential retrofit onto existing commercial hair dryers. The cylindrical MPP absorber thus offers a practical approach for integrating noise mitigation features without compromising airflow performance or altering the device's ergonomic form factor.

Table 2: Overall SWL at high fan speed with different attachments

Attachment Type	without Absorber (dB(A))	with Absorber (dB(A))	Reduction (dB(A))
No attachment	87.38	85.23	2.15
ThermoProtect	86.77	85.60	1.17
Styling Nozzle	86.13	84.83	1.30
Diffuser	87.57	86.53	1.04

Following the design, fabrication, and installation of the MPP-based sound absorber at the air inlet of the hair dryer, sound level measurements were repeated under four operating conditions: without any attachment, with the ThermoProtect attachment, with the styling nozzle, and with the diffuser. The results of these measurements are presented in Table 2, which compares the A-weighted SPL values before and after the MPP based sound absorber installation. The inclusion of the MPP absorber led to noticeable reductions in SPL across all configurations. In the no attachment scenario, the SPL decreased from 87.38 dB(A) to 85.23 dB(A), indicating a reduction of 2.15 dB(A). This scenario, in which the air inlet is most exposed, demonstrated the greatest benefit from the absorber, supporting the design decision to focus noise mitigation efforts on the inlet side. In the ThermoProtect and styling nozzle configurations, SPL reductions of 1.17 dB(A) and 1.30 dB(A) were observed, respectively. The diffuser configuration, although exhibiting the highest baseline SPL at 87.57 dB(A), also showed the smallest improvement of 1.04 dB(A), likely due to outlet-side flow disturbances dominating the overall acoustic output.

Overall, these results confirm that the MPP absorber, while compact and non-invasive, delivers consistent noise attenuation under practical use conditions. The reduction of 2.15 dB(A) for no attachment, while moderate, are acoustically significant—particularly in consumer product contexts where even a 1–2 dB(A) reduction can lead to a perceptible improvement in user comfort. Furthermore, the absorber did not adversely affect airflow or thermal performance,

preserving the hair dryer's functional integrity. The findings affirm the effectiveness of passive noise control using a perforated absorber and demonstrate the potential of localized, inlet-focused treatments for compact appliances where traditional damping materials may not be feasible. Future improvements may include combining the perforated absorber with upstream flow-straightening or damping structures to further suppress turbulent noise at both the inlet and outlet ends.

4. CONCLUSION

This study successfully achieved its objective of designing, simulating, fabricating, and evaluating a perforated sound absorber for reducing the noise generated by a hair dryer. Initial SWL measurements were conducted on a commercial hair dryer at both high and low fan speeds, with and without attachments. The highest SWL readings were observed during high-speed operation, ranging from 85.88 dBA to 87.57 dBA depending on the attachment, confirming that high fan speed represented the most acoustically critical condition. Based on these measurements, a range of perforated parameters was proposed within the constraints of design and application. SAC simulations were carried out, and the optimal MPP parameters were identified. This design was chosen for fabrication due to its practical manufacturability and strong simulated performance.

A small scale MPP sample was fabricated using FDM 3D printing with PLA filament. It was then validated through SAC measurements using a two-microphone impedance tube method, following ISO and ASTM standards. The experimental SAC closely matched the simulation trend, with peak frequencies aligning well. Minor discrepancies were attributed to fabrication tolerances and slight irregularities in the printed perforations. The validated MPP was then applied to the hair dryer, and the overall SWL was measured again under the same operating conditions. This method showed promise for consumer appliance manufacturers aiming to reduce noise without major redesign. The results showed a consistent noise reduction across all attachment configurations, with the highest reduction being 2.15 dBA (no attachment), demonstrating the effectiveness of the MPP in mitigating hair dryer noise.

In conclusion, the integration of simulation-driven design and additive manufacturing enabled the development of an acoustically effective perforated sound absorber solution. This work highlights the potential of a sound absorber as a lightweight, compact, and customizable approach for targeted noise control in consumer appliances.

ACKNOWLEDGEMENT

The authors would like to "Ministry of Higher Education Malaysia for Fundamental Research Grant Scheme with Project Code: FRGS/1/2023/TK10/USM/02/2.

REFERENCES

Akhmetov, B., Gupta, S., & Ahuja, K. K. (2014). Noise source ranking of a hairdryer (Paper No. AIAA 2014-3184). 20th AIAA/CEAS Aeroacoustics Conference, Atlanta, GA. https://doi.org/10.2514/6.2014-3184.

Alisah, M. I., Ooi, L. E., Ripin, Z. M., Yahaya, A. F. & Ho, K. (2021). Acoustic attenuation performance analysis and optimisation of expansion chamber coupled micro-perforated cylindrical panel using response surface method. *Archives of Acoustics*, 46(3), 507–517. https://doi.org/10.24425/aoa.2021.138143

ASTM International. ASTM E1050: Standard test method for impedance and absorption of acoustical materials using a tube, two microphones and a digital frequency analysis system.

Azimi, M. & Ommi, F. (2014) Fan noise sources and passive reduction methodologies in high bypass turbofan engines. *Noise and Vibration Worldwide*, 45(5). https://doi.org/10.1260/0957-4565.45.5.18.

Cawser, S. (2019). Acoustic measurements in airflow. Acoustics Bulletin, 44(2), 28–30. Institute of Acoustics.

Carbajo, J., Nam, S. H. & Fang, N. X. (2024) Fabrication of Micro-Perforated Panel (MPP) sound absorbers using Digital Light Processing (DLP) 3D printing technology. Applied Acoustics, 216, 109788.

Che, L., Lee, H. M., & Lee, H. P. (2024). Acoustical analysis and optimization design of the hair dryers. Noise Mapping, 11(1), 20240004. https://doi.org/10.1515/noise-2024-0004

Gao, N. & Hou, H. (2018) Sound absorption characteristic of micro-helix metamaterial by 3D printing. Theoretical and Applied Mechanics Letters, 8(2), 63-67.

Gupta, S., Akhmetov, B., & Ahuja, K. K. (2014). Creative means of making acoustic measurements inexpensively with hair dryer noise reduction as an example (Paper No. AIAA/CEAS-2014-3185). 20th AIAA/CEAS Aeroacoustics Conference, Atlanta, GA. https://doi.org/10.2514/6.2014-3185.

Herrin, D. & Liu, J. (2011) Properties and Applications of Microperforated Panels. Sound and Vibration

Herrin,D., Liu, W., Hua, X. &, Liu, J. (2017) A Guide to the Application of Microperforated Panel Absorbers. Sound and Vibration.

Huang, Y., & Zheng, Q. (2022). Sound quality modelling of hairdryer noise. Applied Acoustics, 197, 108896.

International Organization for Standardization. (2010). ISO 3741:2010 Acoustics — Determination of sound power levels and sound energy levels of noise sources using sound pressure — Precision methods for reverberation test rooms (4th ed.).

International Organization for Standardization. (2016). *ISO 3745:2012 Acoustics — Determination of sound power levels and sound energy levels of noise sources using sound pressure — Precision methods for anechoic rooms and hemi-anechoic rooms* (3rd ed.).

István, L. V. & Leo, L. B. (2005). Noise and Vibration Control Engineering: Principles and Applications. Wiley Inter-Science, Hoboken.

Jafar, N. A., Ooi, L. E., Mazlan, A. Z. A., Seng, K. H. C., & Tan, J. M. (2020). The evaluation of deviation in sound absorption coefficient for micro-perforated panel. In IOP Conference Series: Materials Science and Engineering, 815 (1), 012009. https://doi.org/10.1088/1757-899X/815/1/012009

Jafar, N. A., Ooi, L. E., Ripin, Z. M., Ho, K. & Yahaya, A. F. (2021). Resistance end correction factor of microperforated panel made using additive manufacturing. *Engineering Science and Technology, an International Journal*, 24(6), 1281-1291.

Lahaye, L. (2022). Hair dryer aero-acoustic study and passive solutions for noise reduction – Integration internship [Master's thesis, Université de Liège].

Liu, Z., Zhan, J., Fard, M. & and Davy, J. L. (2017). Acoustic measurement of a 3D printed micro-perforated panel combined with a porous material. Measurement, 104, 233–236.

Liu, Z., Zhan, J., Fard, M. & and Davy, J. L. (2017) Acoustic properties of multilayer sound absorbers with a 3D printed micro-perforated panel, Applied Acoustics, 121, 25-32.

Mohamed Shafeer, P. P., Pitchaimani, J. & Doddamani, M. (2024) 3D Printed Thick Micro-Perforated Panel with Graded Perforation for Practical Wall Sound Absorption Applications. *Acoustics Australia*, 52(1), 25-40.

Münzel, T., Gori, T., Babisch, W., & Basner, M. (2014). Cardiovascular effects of environmental noise exposure. European heart journal, 35(13), 829–836. https://doi.org/10.1093/eurheartj/ehu030.

National Institute for Occupational Safety and Health (NIOSH), Criteria for a Recommended Standard: Occupational Noise Exposure (NIOSH, Cincinnati, 1998.

Nicolo Altamore (1999). Hair drying device with reduced sound emissions. U.S. Patent No US6148537A.

Petersen, E. C.. An overview of standards for sound power determination (Application Note BO 0416-12). Bruel & Kjær. https://www.bksv.com/doc/bo0416.pdf

Qian, Y. J., Kong, D. Y., Liu, S. M, Sun, S. M. & Zhao, Z. (2013). Investigation on micro-perforated panel absorber with ultra-micro perforations. Applied Acoustics, 74(7), pp. 931–935. doi: 10.1016/j.apacoust.2013.01.009.

Rafique, F., Wu, J. H., Chong, R. L. & Ma, F. (2022) Transmission Loss analysis of a simple expansion chamber muffler with extended inlet and outlet combined with inhomogeneous micro-perforated panel (iMPP). *Applied Acoustics*, 194, 108808. https://doi.org/10.1016/j.apacoust.2022.108808.

Rodrigues, O. J. (2010, April 29). Electrical hair dryer with noise reducer and noise reducer (Patent No. WO 2010045698A1). World Intellectual Property Organization.

Sailesh, R., Yuvaraj, L., Pitchaimani, J., Doddamani, M. & Mailan Chinnapandi, L. B. (2021) Acoustic behaviour of 3D printed bio-degradable micro-perforated panels with varying perforation cross-sections, Applied Acoustics, 174 107769.

Sailesh, R., Yuvaraj, L., Doddamani, M., Mailan Chinnapandi, L. B. & Pitchaimani, J. (2022) Sound absorption and transmission loss characteristics of 3D printed bio-degradable material with graded spherical perforations, Applied Acoustics, 186, 108457.

Sakagami, K., Kusaka, M., Okuzono, T., Kido, S., & Yamaguchi, D. (2021). Application of transparent microperforated panels to acrylic partitions for desktop use: A case study by prototyping. UCL Open Environment, 2. https://doi.org/10.14324/111.444/ucloe.000021.

Sathyan, S., Aydin, U., & Belahcen, A. (2020). Acoustic noise computation of electrical motors using the boundary element method. *Energies, 13*(1), 245. https://doi.org/10.3390/en13010245.

Wareing, R. R., Davy, J. L. & Pearse, J. R. (2015) Predicting the sound insulation of plywood panels when treated with decoupled mass loaded barriers. Applied Acoustics, 91, 64–72.

